Icarus 296 (2017) 99–109

Contents lists available at ScienceDirect

Icarus

journal homepage: www.elsevier.com/locate/icarus

# Stability of ice on the Moon with rough topography

Lior Rubanenko[a,b,*], Oded Aharonson[b]

[a] Department of Earth, Planetary and Space Sciences, UCLA, 595 Charles E Young Dr E, Los Angeles, CA 90095, USA
[b] Weizmann Institute of Science, Rehovot, 7610001, Israel

ARTICLE INFO

*Article history:*
Received 8 October 2016
Revised 24 April 2017
Accepted 31 May 2017
Available online 31 May 2017

*Keywords:*
Ices
Moon
Surface
Regoliths
Solar radiation

ABSTRACT

The heat flux incident upon the surface of an airless planetary body is dominated by solar radiation during the day, and by thermal emission from topography at night. Motivated by the close relationship between this heat flux, the surface temperatures, and the stability of volatiles, we consider the effect of the slope distribution on the temperature distribution and hence prevalence of cold-traps, where volatiles may accumulate over geologic time. We develop a thermophysical model accounting for insolation, reflected and emitted radiation, and subsurface conduction, and use it to examine several idealized representations of rough topography. We show how subsurface conduction alters the temperature distribution of bowl-shaped craters compared to predictions given by past analytic models. We model the dependence of cold-traps on crater geometry and quantify the effect that while deeper depressions cast more persistent shadows, they are often too warm to trap water ice due to the smaller sky fraction and increased reflected and reemitted radiation from the walls. In order to calculate the temperature distribution outside craters, we consider rough random surfaces with a Gaussian slope distribution. Using their derived temperatures and additional volatile stability models, we estimate the potential area fraction of stable water ice on Earth's Moon. For example, surfaces with slope RMS ~15° (corresponding to length-scales ~10 m on the lunar surface) located near the poles are found to have a ~10% exposed cold-trap area fraction. In the subsurface, the diffusion barrier created by the overlaying regolith increases this area fraction to ~40%. Additionally, some buried water ice is shown to remain stable even beneath temporarily illuminated slopes, making it more readily accessible to future lunar excavation missions. Finally, due to the exponential dependence of stability of ice on temperature, we are able to constrain the maximum thickness of the unstable layer to a few decimeters.



## 1. Introduction

The small obliquity of airless planetary bodies such as the Moon and Mercury causes topographic depressions located near their poles to be in permanent or near-permanent shadow for geologic time periods. Previous works (*e.g.* Watson et al., 1961) have shown that the lifetime of volatile deposits residing within those cold-traps is comparable to the lifetime of bodies in the Solar System.

The cold-trap distribution is tightly linked to the temperature distribution on and below the surface, which itself is governed by the shape of the topography controlling the abundance of shadows and the amount of radiation reaching them. To a lesser extent, it is also a function of the thermal properties controlling conduction into the subsurface. The latter can be modeled by solving the 1D heat diffusion equation (Schorghofer and Aharonson, 2005; Aharonson and Schorghofer, 2006). The former has been modeled assuming the topography consists of spherical craters (Buhl et al., 1968; Ingersoll et al., 1992; Hayne and Aharonson, 2015) or of normally distributed slopes (Smith, 1967; Bandfield et al., 2015) to which an analytic solution exists. In the past two decades more general models have been developed utilizing algorithms such as ray casting and ray tracing (Paige et al., 1992; Vasavada et al., 1999; Davidsson and Rickman, 2014), combined with subsurface heat conduction. Using those models, cold-traps were shown to exist near the poles of the Moon and Mercury. Later, temperatures characteristic of cold-traps (Paige et al., 2010b) and direct evidence for frozen volatiles deposits were discovered (Colaprete et al., 2010) on the Moon as well as remotely sensed on Mercury in RADAR (Harmon et al., 2001), laser altimetry (Neumann et al., 2013; Paige et al., 2013) and visible imagery (Chabot et al., 2014).

* Corresponding author at: Department of Earth, Planetary and Space Sciences, UCLA, 595 Charles E Young Dr E, Los Angeles, CA 90095, USA.
*E-mail address:* liorr@ucla.edu (L. Rubanenko).

http://dx.doi.org/10.1016/j.icarus.2017.05.028
0019-1035/

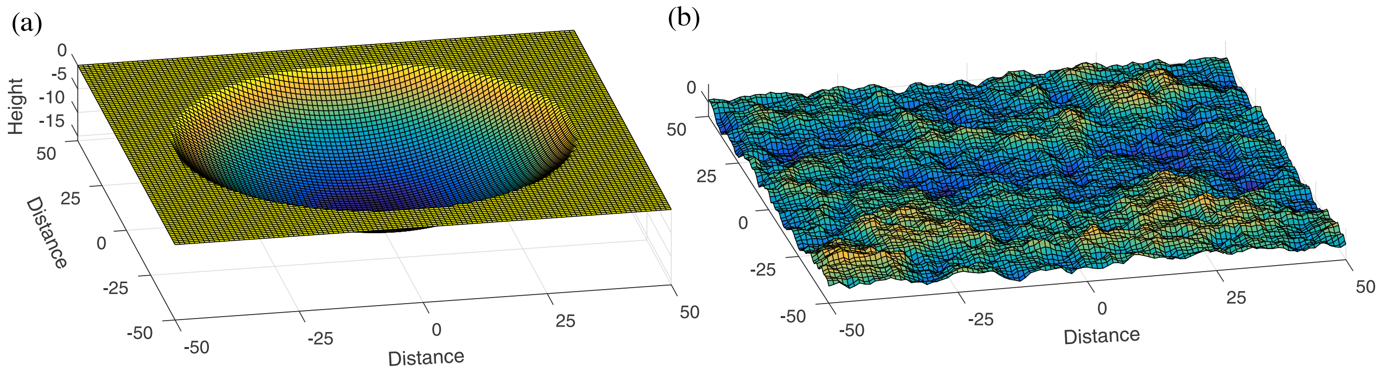


**Fig. 1.** Two examples for the topographies we used in modeling the temperature distribution, visualized in natural units. (a) A spherical crater with depth to diameter $\Delta = 0.2$. (b) A rough random Gaussian surface with a slope RMS $\sigma_s = 15^{\circ}$.

## 2. Models

### 2.1. Roughness models

Here we develop and employ a thermophysical model that accounts for insolation, scattering, thermal emission and subsurface conduction, in order to investigate the link between roughness, temperature and cold-trap stability on and below the lunar surface. We first calculate the temperature distribution of two commonly used, idealized representations of rough topography: a hemispherical (bowl-shaped) crater and a rough random surface with a Gaussian slope distribution. Subsequently, we apply our findings to discuss the stability of surface and subsurface water ice.

#### 2.1.1. Spherical craters

A spherical crater is defined as a cavity shaped as a portion of a sphere of radius $r$, surrounded by a flat plane. The size of the crater is defined by its radius $R$, its depth $h$, or by its depth to diameter ratio, $\Delta = h/2R$. Simple craters with diameters $< 15$ km on the Moon are well approximated by spherical cavities with $\Delta \sim 1/5$ to $\Delta \sim 1/16$ (Pike, 1977; Stopar et al., 2012).

The height of the topography $z$ is given in terms of the horizontal coordinates $x$ and $y$. The equation describing the topography is $z = r - h \pm \sqrt{r^2 - x^2 - y^2}$. An example for a spherical crater with $\Delta = 1/5$ can be seen in Fig. 1a.

#### 2.1.2. Rough random surfaces with a Gaussian slope distribution

A common way to quantify rough terrain on airless bodies outside simple craters is to assume it is random with a Gaussian height and slope distributions (*e.g.* Hagfors, 1964; Smith, 1967; Jamsa et al., 1993; Davidsson and Rickman, 2014; Davidsson et al., 2015; Bandfield et al., 2015), and describe it via the RMS slope magnitude at a given scale, $\sigma_s$. The dependence of the roughness on the 1D lateral scale may be described by a power-law spectrum with an exponent which was measured for the lunar polar regions to be $\sim 2.9$ (Rosenburg et al., 2011; Schroeder, 2012). In our model, $\sigma_s$ is computed at the facet scale. Different values of $\sigma_s$ may be regarded as corresponding to different scales on the Moon (Rosenburg et al., 2011). Therefore, in our discussion of ice stability we specify in addition to the RMS slope, the scale that corresponds to this value according to measurements of the lunar surface. These random surfaces could be used to explore topographies in scales lower than the instrument resolution (*e.g.*, Rubanenko et al., 2017).

In order to construct the model surface, we seed a matrix with a 2D Gaussian random field with a unity standard deviation and zero mean. This field has white spectrum. We compute the 2D discrete Fourier transform of the matrix and multiply its magnitude by a power-law weight function in wave number, shaping its power spectrum to the desired form. We smoothly truncate the coefficients of the highest 20% of the wavenumbers to avoid unrealistic discontinuities in the field. To obtain the surface elevation map we compute the inverse discrete Fourier transform and scale its overall magnitude to obtain the desired RMS slope at the pixel scale. This results in a height distribution with a normally distributed magnitude and uniformly distributed phase (Wu, 2000). The resulting surface directional slopes are Gaussian distributed, bi-directional slope magnitudes are Rayleigh distributed with slope aspects uniformly distributed. An example for a random rough surface with these properties can be seen in Fig. 1b.

### 2.2. Thermophysical model

In order to isolate the different variables that determine the surface and subsurface temperature of airless bodies, we have constructed a thermophysical illumination model. As mentioned above, this has been accomplished by employing different methods, usually involving a versatile illumination algorithm combined with a heat conduction model into the subsurface (*e.g.*, Paige et al., 1992; Salvail and Fanale, 1994; Lagerros, 1997; Davidsson and Rickman, 2014). Our improved model includes a highly efficient illumination algorithm and an implicit subsurface heat conduction model, allowing us to achieve convergence in the subsurface temperatures using only few integration time steps.

#### 2.2.1. Shadowing and multiple scattering

The Sun is the primary energy source for many airless bodies in the Solar System as the geothermal energy flux can usually be neglected. To estimate the intensity of incident radiation, we start with a topography represented by a matrix of size $N \times N$ square facets of equal area, denoted by their linear index $i$ assuming values between 1 and $N^2$. For both the spherical craters and Gaussian random surfaces we choose $N = 100$.

For simplicity, the solar flux is computed as from a point source, smoothed in time (see Section 2.3). Other approaches (*e.g.*, Davidsson and Rickman, 2014) scale the flux received by a facet by the fraction of its vertices that are illuminated. We expect this correction to be important only near the shadow edges, therefore we consider an error of 1 pixel when determining the flux reaching pixels located in those areas.

In order to simulate shadows and reflections from the surface we adopt the Ray Casting technique (Roth, 1982). Virtual light rays are cast as probes in all directions, and their intersection points with other objects are used in order to determine the objects scale and distance from one another. This method is relatively simple but computationally intensive due to the need to find all surface-line intersections. Using predefined geometrical shapes may reduce